Supporting Information

Elucidating the mechanism of the CO_2 methanation reaction over Ni-Fe hydrotalcite-derived catalysts via surface-sensitive *in situ* XPS and NEXAFS

Gianfranco Giorgianni,[a] Chalachew Mebrahtu,[b] Manfred Erwin Schuster,[c] Alexander Ian Large,[d] Georg Held,[d,e] Pilar Ferrer,[e] Federica Venturini,[e] David Grinter,[e] Regina Palkovits,[b] Siglinda Perathoner,[f] Gabriele Centi,[g] Salvatore Abate*[f] and Rosa Arrigo *[e,h]

Experimental Protocol

Table S 1: Experimental protocol (all catalytic tests have been performed at 300 °C)

Cat.	Cat. Pre-treatment	Test #	H_2 (mbar)	CO_2 (mbar)	H_2O (mbar)
Ni/HT	Pre-reduced. 1) Ramp 25-500 °C (5 °C/min) at 1 mbar H_2 2) Isotherm at 500 °C for 8 h	1	1.2	0.3	0
	None	2	2.4	0.6	0
	None	3	1.8	0.45	0.75
	Reduced again. 1) 300-500 °C, 18 mbar H_2 2) Isotherm at 500 °C, 2 mbar H_2, 3 h	4	2.4	0.6	0
	Reduced again: 1) 300-500 °C, 18 mbar H_2 2) Measurement in H_2O 3) 300-500 °C, 3 mbar, H_2 0.5 h	5	1.2	0.3	1.5
Ni-Fe/HT	Pre-reduced. 1) Ramp 25-500 °C (10 °C/min) at 1 mbar H_2 2) Isotherm at 500 °C and 1 mbar H_2 for 5 h 3) Isotherm at 500 °C and 2 mbar for 2 h	1	1.2	0.3	0
	None	2	2.4	0.6	0
	None	3	1.8	0.45	0.75
	Fresh, Pre-reduced 1) 300-500 °C at 10 mbar H_2 2) isotherm 500 °C, 5 mbar H_2 for 2 h	4	2.4	0.6	0
	None	5	1.2	0.3	1.5

Equations for the calculation of conversion, selectivity, and yield toward methane

$$Conversion_{CO_2} = \frac{(pCH_{4_{Measured}} + pCO_{Measured})}{pCO_{2_{Set}}} \quad (1)$$

$$Conversion_{H_2} = \frac{(2 \cdot pCH_{4_{Measured}} + pH_2O_{Measured} - pH_2O_{Set})}{pH_{2_{Set}}} \quad (2)$$

$$Selectivity_{CH_4} = \frac{pCH_{4_{Measured}}}{(pCH_{4_{Measured}} + pCO_{Measured})} \quad (3)$$

$$Selectivity_{\mathrm{CO}} = \frac{pCO_{Measured}}{(pCH_{4_{Measured}} + pCO_{Measured})} \quad (4)$$

$$Selectivity_{CH_4}, = \frac{pCH_{4_{Measured}}}{pCO_{Measured}} \quad (5)$$

$$Yield_{CH_4} = Selectivity_{CH_4} \cdot Conversion_{CO_2} \quad (6)$$

$$Yield_{CO} = Selectivity_{CO} \cdot Conversion_{CO_2} \quad (7)$$

$$s = \sqrt{\sum_{i=1}^{N} \frac{(x_i - \bar{x})^2}{N-1}} \quad (8)$$

Where *x* is the value of the measured data point and *N* is the number of data points.

Calculation of partial pressures from MS online measurements

To determine the catalysts´ performances, the mass signal *m/z* 2, 14, 15, 16, 18, 28, 40 and 44 were monitored by means of an online mass spectrometer.
The experimental mass signal measured as a function of time for each analysed ion (n), Mn where, $n = [2, 14, 15, 16, 18, 28, 40, 44]$, was linearized and normalized according to the equation

$$Mn_{exp} = \frac{10^{Mn}}{\sum_n 10^{Mn}}. \quad (9)$$

The partial pressure of the gases H_2, CO_2, CO, CH_4 and H_2O in the reaction mixture of each experiment were obtained from the relevant experimental mass signals *Mn* by minimizing the difference between the *experimental spectrum* and a *simulated spectrum*. The simulated spectrum for each mass fragment *m/z* was obtained by convoluting the theoretical contributions to the *m/z* signal of the various gases in the reaction mixture as found in the NIST database.

It was assumed that the convoluted mass spectra at each point in time is given by the relative intensity of each mass fragment multiplied by the molar fraction $y_{Component}$ ($component = H_2, CH_4, CO, CO_2, H_2O, Ar, N_2$) as reported in the following functions.

$$M2(y_{H_2}, y_{CH_4}, y_{CO}, y_{CO_2}, y_{H_2O}, y_{Ar}, y_{N_2}) = 100y_{H_2}$$
$$M14(y_{H_2}, y_{CH_4}, y_{CO}, y_{CO_2}, y_{H_2O}, y_{Ar}, y_{N_2}) = 20.4y_{CH_4} + 4.55y_{N_2}$$
$$M15(y_{H_2}, y_{CH_4}, y_{CO}, y_{CO_2}, y_{H_2O}, y_{Ar}, y_{N_2}) = 88.7y_{CH_4}$$
$$M16(y_{H_2}, y_{CH_4}, y_{CO}, y_{CO_2}, y_{H_2O}, y_{Ar}, y_{N_2}) = 9.52y_{CO_2} + 100y_{CH_4}$$
$$M18(y_{H_2}, y_{CH_4}, y_{CO}, y_{CO_2}, y_{H_2O}, y_{Ar}, y_{N_2}) = 100y_{H_2O}$$
$$M28(y_{H_2}, y_{CH_4}, y_{CO}, y_{CO_2}, y_{H_2O}, y_{Ar}, y_{N_2}) = 100y_{CO} + 9.75y_{CO_2} + 100y_{N_2}$$
$$M40(y_{H_2}, y_{CH_4}, y_{CO}, y_{CO_2}, y_{H_2O}, y_{Ar}, y_{N_2}) = 100y_{Ar}$$

$$M44(y_{H_2}, y_{CH_4}, y_{CO}, y_{CO_2}, y_{H_2O}, y_{Ar}, y_{N_2}) = 100 y_{CO_2}$$
$$Sum(y_{H_2}, y_{CH_4}, y_{CO}, y_{CO_2}, y_{H_2O}, y_{Ar}, y_{N_2}) = \sum_n M_n(y_{H_2}, y_{CH_4}, y_{CO}, y_{CO_2}, y_{H_2O}, y_{Ar}, y_{N_2})$$

The composition in terms of molar fractions of each component was obtained by minimizing the following objective function:

$$ObjFun(y_{H_2}, y_{CH_4}, y_{CO}, y_{CO_2}, y_{H_2O}, y_{Ar}, y_{N_2}, M2_{exp}, M14_{exp}, M15_{exp}, M16_{exp}, M18_{exp}, M28_{exp}, M40_{exp}, M44_{exp}) = \sum_n \left(Mn_{exp} - \frac{Mn(y_{H_2}, y_{CH_4}, y_{CO}, y_{CO_2}, y_{H_2O}, y_{Ar}, y_{N_2})}{Sum(y_{H_2}, y_{CH_4}, y_{CO}, y_{CO_2}, y_{H_2O}, y_{Ar}, y_{N_2})} \right)^2 \quad (10)$$

To get the composition trend, the objective function was minimized for each point in time with respect to the composition ($y_{H_2}, y_{CH_4}, y_{CO}, y_{CO_2}, y_{H_2O}, y_{Ar}, y_{N_2}$) after imposing the following constraints:

$$y_{Component} \geq 0$$

$$\sum_{Component} y_{Component} = 1$$

The whole algorithm was programmed in Wolfram Mathematica 11.3.
The objective function was minimized by using the $N_{Minimize}$ method.
The partial pressures of each component were obtained by the following equations

$$p_{Component} = y_{Component} P_{total} \quad (11)$$

P_{total} is the total pressure set for the APXPS chamber (mbar).
The conversion, selectivity and yield to methane were measured by the equations 1-7.

Table S 2: Calculated average partial pressures as determined by applying eq. (10)-(11).

Catalyst	Test	Operating Conditions	Avg. pH_2 (mbar)	Avg. CO_2 (mbar)	Avg. H_2O (mbar)	Avg. CH_4 (mbar)	Avg. CO (mbar)
Ni/HT	1	$H_2/CO_2/H_2O$, 1.2/0.3/0 mbar	1.17	0.21	0.09	0.01	0.03
	2	$H_2/CO_2/H_2O$, 2.4/0.6/0 mbar	2.52	0.30	0.16	0.03	0.05
	3	$H_2/CO_2/H_2O$, 1.8/0.45/0.75 mbar	2.01	0.27	0.64	0.02	0.03
	4	$H_2/CO_2/H_2O$, 2.4/0.6/0 mbar	2.24	0.30	0.29	0.11	0.11
	5	$H_2/CO_2/H_2O$, 1.2/0.3/1.5 mbar	1.09	0.16	1.60	0.03	0.02
Ni-Fe/HT	1	$H_2/CO_2/H_2O$, 1.2/0.3/0 mbar	1.10	0.19	0.11	0.04	0.04
	2	$H_2/CO_2/H_2O$, 2.4/0.6/0 mbar	2.44	0.24	0.24	0.11	0.03
	3	$H_2/CO_2/H_2O$, 1.8/0.45/0.75 mbar	2.16	0.17	0.76	0.03	0.02
	4	$H_2/CO_2/H_2O$, 2.4/0.6/0 mbar	2.28	0.31	0.24	0.07	0.09
	5	$H_2/CO_2/H_2O$, 1.2/0.3/1.5 mbar	1.15	0.32	1.58	0.03	0.02

Table S 3: Calculated standard deviation *S* using the formula (8).

Catalyst	Conditions	*S* Conversion CO_2	*S* CH_4 Selectivity	*S* CH_4 yield
Ni-Fe/HT	Test 1, $H_2/CO_2/H_2O$ 1.2/0.3/0 mbar	1,60%	1,50%	0,50%
	Test 2, $H_2/CO_2/H_2O$ 2.4/0.6/0 mbar	2,10%	0,70%	1,60%
	Test 3, $H_2/CO_2/H_2O$ 1.8/0.45/0.75 mbar	2,00%	0,80%	1,00%
Ni-Fe/HT	Test 4, $H_2/CO_2/H_2O$ 2.4/0.6/0 mbar	2,80%	3,60%	1,10%
	Test 5, $H_2/CO_2/H_2O$ 1.5/0.3/1.5 mbar	1,20%	1,00%	0,40%
Ni/HT	Test 1, $H_2/CO_2/H_2O$ 1.2/0.3/0 mbar	1,00%	3,00%	0,00%
	Test 2, $H_2/CO_2/H_2O$ 2.4/0.6/0 mbar	1,20%	1,60%	0,40%
	Test 3, $H_2/CO_2/H_2O$ 1.8/0.45/0.75 mbar	0,70%	2,30%	0,30%
	Test 4, $H_2/CO_2/H_2O$ 2.4/0.6/0 mbar	1,50%	1,50%	0,70%
	Test 5, $H_2/CO_2/H_2O$ 1.5/0.3/1.5 mbar	1,00%	0,80%	0,50%

Fitting of Ni2p XPS

The fittings of the Ni2p spectra were performed by applying consistently a model that includes core-level components with line shape obtained from a previous study on Ni nanoparticles (see references in the main text). The spectra were fitted following the Levenberg-Marquardt algorithm to minimize the residual standard deviation. A Doniach–Šunjić (DS) function line-shape was used for the metallic Ni1 components at 852.6 eV and for Ni2 at 853.7 eV. A Ni3 components with a Gaussian-Lorentzian (GL) line-shape at *ca.* 855.8 eV was included accounting for Ni^{2+}/Ni^{3+} oxyhydroxide species. With respect to our previous work, an additional Ni4 component with a Gaussian-Lorentzian (GL) line-shape was required at a fixed energy of 859.1 eV to afford a good fitting. A Similar BE was reported for mixed oxides containing Ni, and therefore, we consider this a Ni aluminate species. The fitting of the spectra was done by fixing the peak position for Ni1, Ni2 and Ni4 whereas for Ni3 it was necessary to constrain the peak position by ± 0.05 eV. The full width at half maximum (FWHM) was fixed to a given value for all the core level as summarized in Table S4, except for the satellite peaks relative to Ni3 and Ni4, for which more flexibility was required. The peak area ratio between the $Ni2p_{3/2}$ and $Ni2p_{1/2}$ spin-orbit split transitions was constrained approximately to the theoretical value of 2:1 and the distance between the two-spin orbit split transition was 17.3 eV. Binding energies (BEs) were referenced to the Fermi level measured after every core level measurement at the same excitation energy. The satellite feature for Ni^0 is 5.7 eV upshift with respect to the core level; its intensity is ca. 30% of the main peak. Satellite peaks related to the Ni3 components were included at a fixed BE of 861.3 eV, 864 eV accounting for *ca.* 50% and 30% of the main peak intensity, respectively. A satellite related to the Ni4 component was found at 867.3 eV with an intensity of 60% of the main peak. These satellites account also for those related to the Ni2 peak which are omitted in the fitting. Whilst, the sample preparation was optimized to by-

pass charging issues, we note that in few cases a low BE tail of the peak could be related to this phenomenon, however this can be safely disregarded.

Table S 4: Ni2p XPS fitting parameters

	Ni1	Ni2	Ni1/Ni2 satellites	Ni3	Ni3 satellites	Ni4	Ni4 satellites
BE (eV)	852.6	853.7	+ 5.7 eV	855.8±0.05	861.3 879.1	859.1	867.3
FWHM	1.3	2	3.2	3÷3.2	3.2; 4.4÷5	3	*ca.* 3.5
Line Shape/Area constraints	DS	DS	0.3 x A*	GL(30)	0.5 x A* 0.3 X A*	GL(30)	0.6 x A*

*area relative to the main peak.

HAADF-STEM images and Energy dispersive X-ray elemental mapping

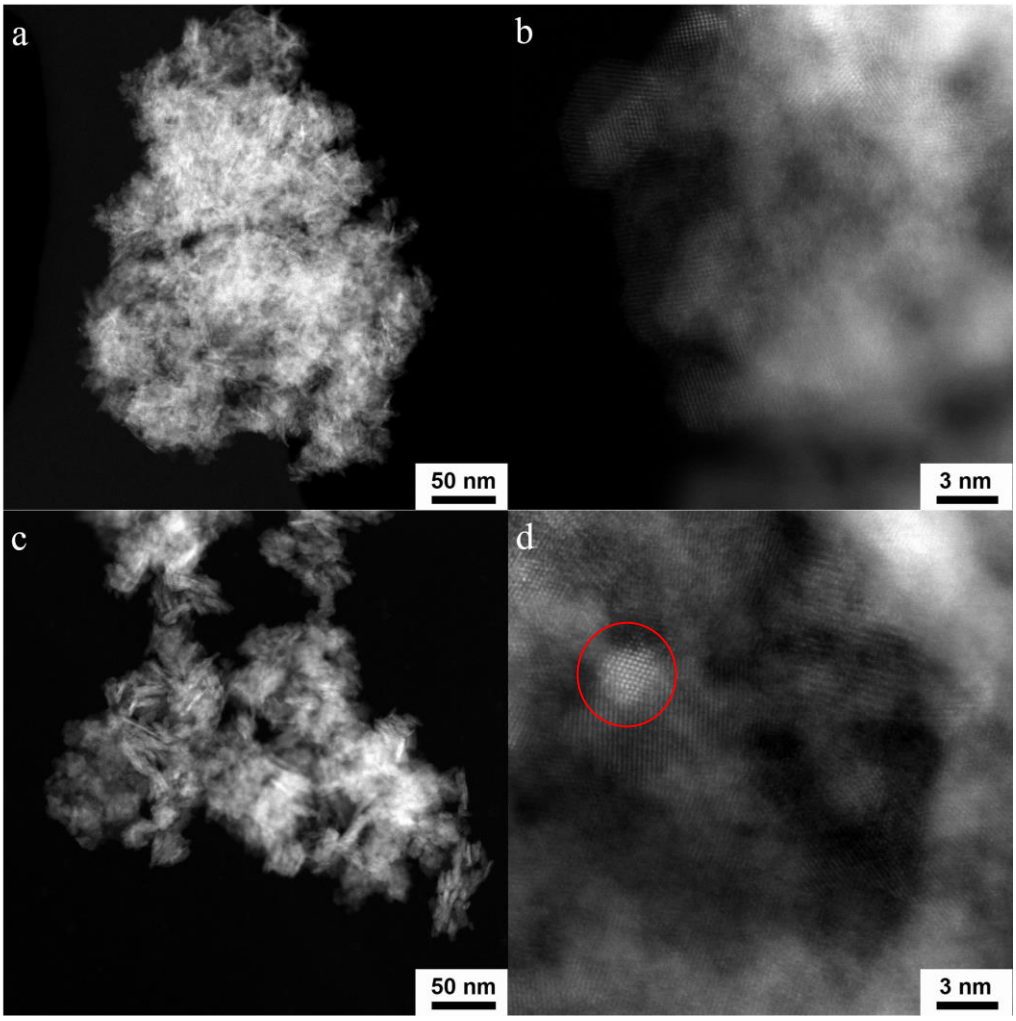

Figure S 1: HAADF-STEM images of Ni-Fe/HT (a and b) and Ni/HT (c and d). Note in the circle in d) a Ni nanoparticle.

a)

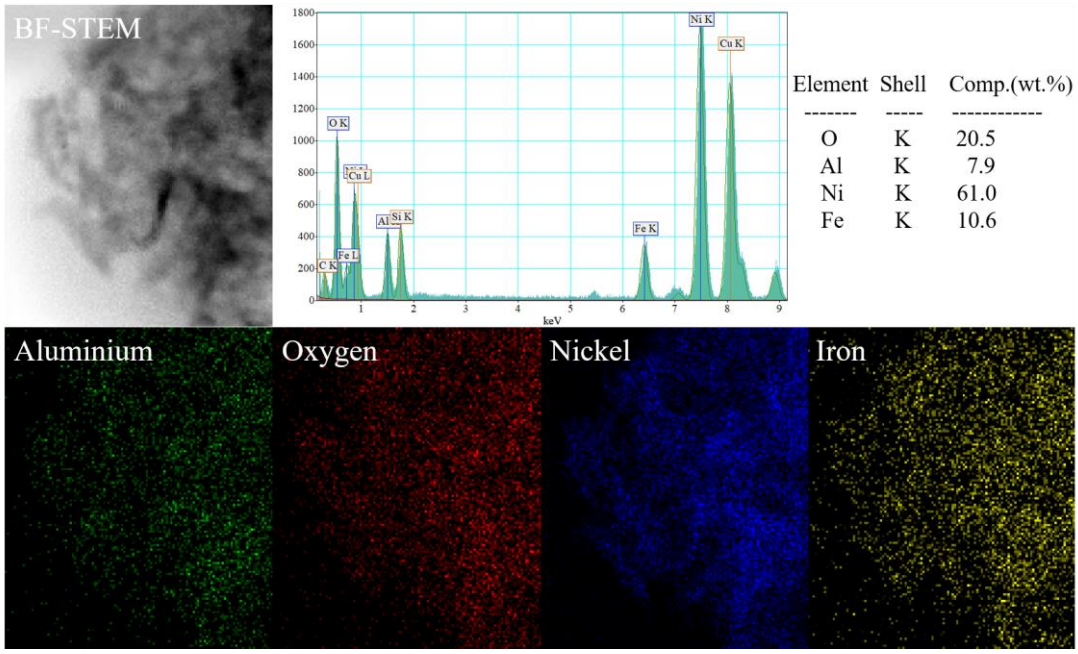

b)

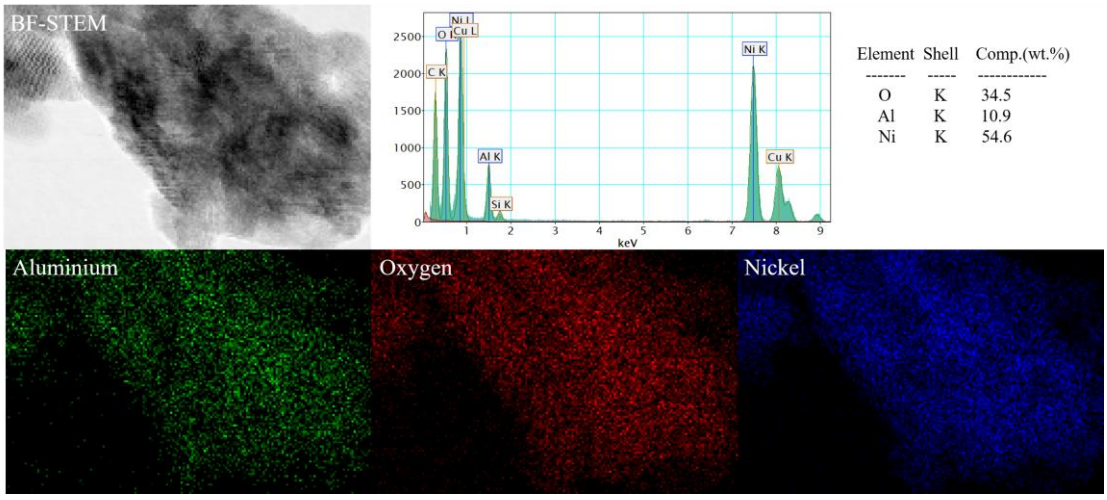

Figure S 2: Energy dispersive X-ray elemental mapping and analysis for Ni-Fe/HT (a) and Ni/HT (b). The quantitative analysis is relatively close to the values found by AAS, where the deviation from them accounts for the amount of C, which cannot be precisely determined by EDX due to the contribution of the C-layer of the TEM grid.

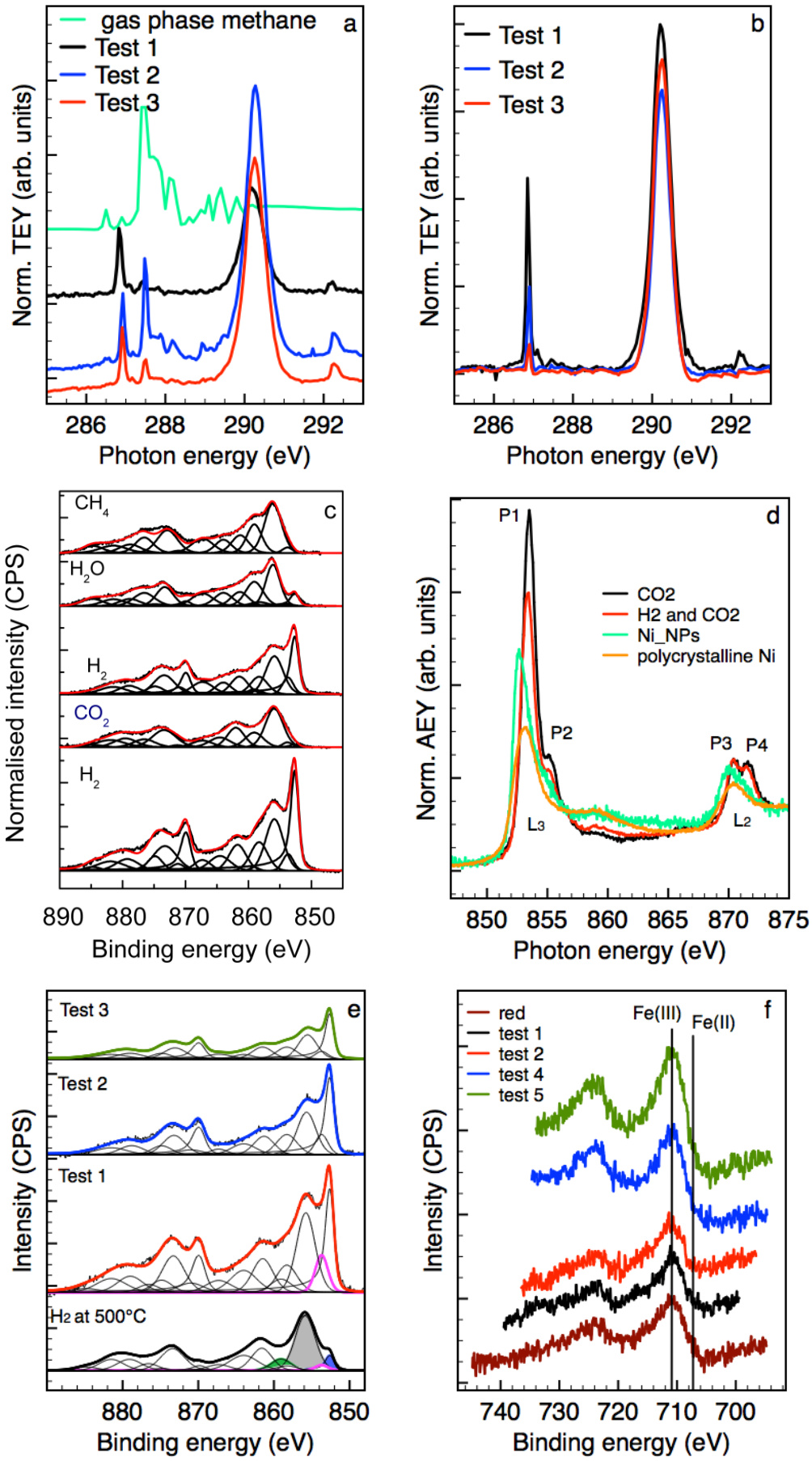
gas phase methane
Test 1
Test 2
Test 3
a
Norm. TEY (arb. units)
286 288 290 292
Photon energy (eV)
b
Test 1
Test 2
Test 3
Norm. TEY (arb. units)
286 288 290 292
Photon energy (eV)
CH4
H2O
H2
CO2
H2
c
Normalised intensity (CPS)
890 880 870 860 850
Binding energy (eV)
P1
P2
P3
P4
L3
L2
d
CO2
H2 and CO2
Ni_NPs
polycrystalline Ni
Norm. AEY (arb. units)
850 855 860 865 870 875
Photon energy (eV)
Test 3
Test 2
Test 1
H2 at 500°C
e
Intensity (CPS)
880 870 860 850
Binding energy (eV)
red
test 1
test 2
test 4
test 5
Fe(III)
Fe(II)
f
Intensity (CPS)
740 730 720 710 700
Binding energy (eV)

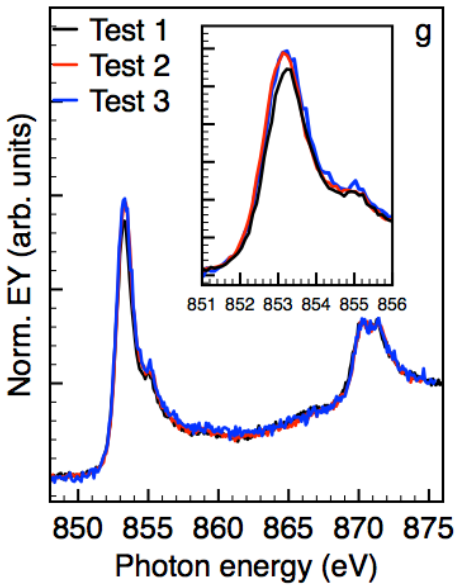
Test 1
Test 2
Test 3
g
Norm. EY (arb. units)
851 852 853 854 855 856
850 855 860 865 870 875
Photon energy (eV)

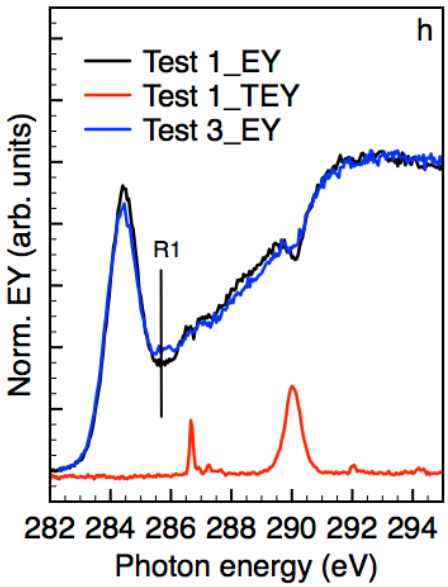
Test 1_EY
Test 1_TEY
Test 3_EY
h
R1
Norm. EY (arb. units)
282 284 286 288 290 292 294
Photon energy (eV)

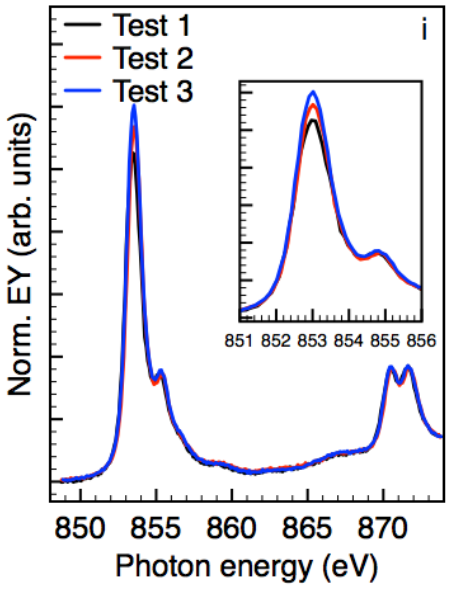
Test 1
Test 2
Test 3
i
Norm. EY (arb. units)
851 852 853 854 855 856
850 855 860 865 870
Photon energy (eV)

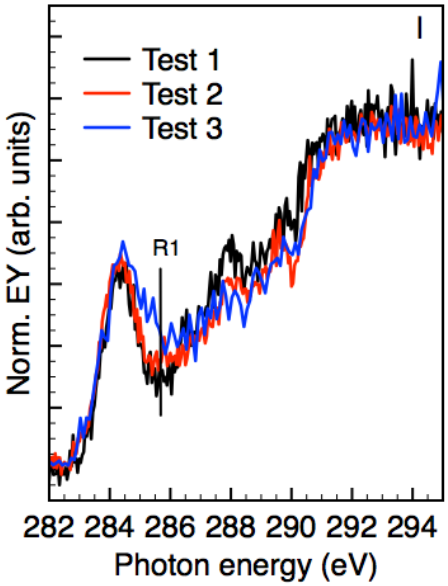
Test 1
Test 2
Test 3
l
R1
Norm. EY (arb. units)
282 284 286 288 290 292 294
Photon energy (eV)

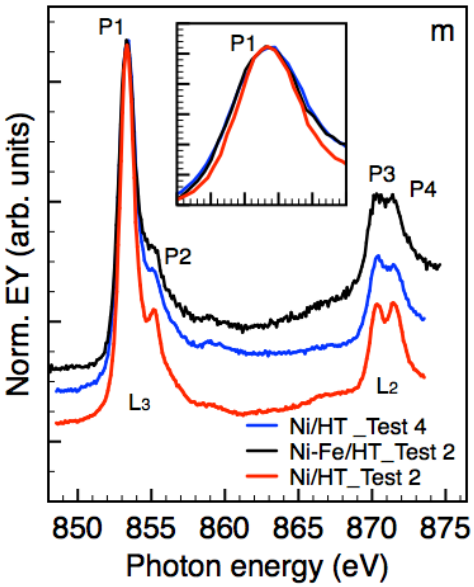
P1
m
P3
P4
P2
L3
L2
Ni/HT _Test 4
Ni-Fe/HT_Test 2
Ni/HT_Test 2
Norm. EY (arb. units)
850 855 860 865 870 875
Photon energy (eV)

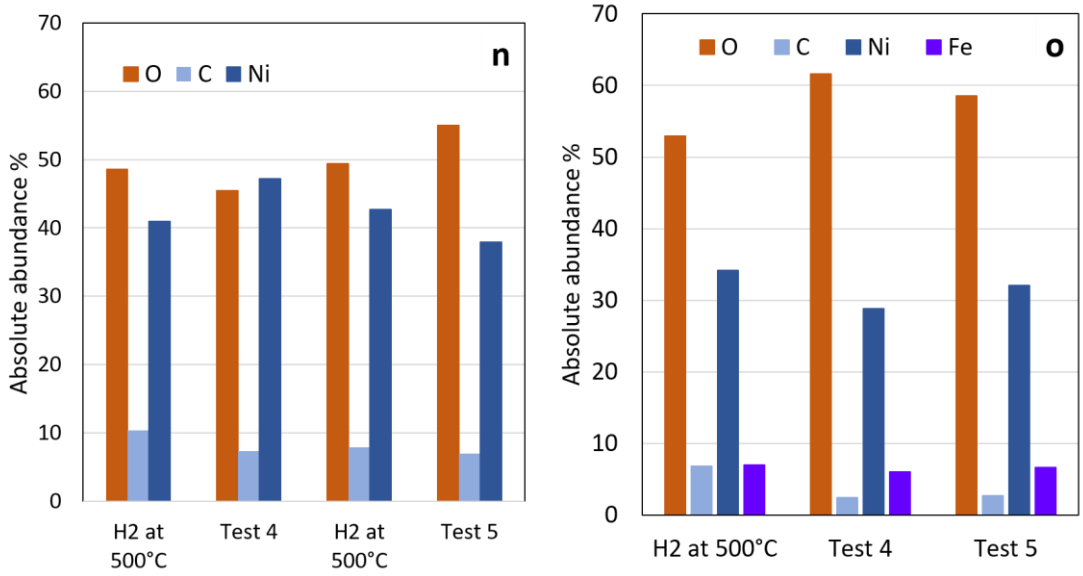

Figure S 3: a) TEY C K-edge NEXAFS of the Ni-Fe/HT under the *in situ* conditions of Fig 2a: in order of increasing energy, the resonances at *ca.* 286.8 eV, 287. 4 eV and 290.3 eV are attributed to gas phase CO, CH_4 and CO_2, respectively; b) TEY C K-edge NEXAFS of the Ni/HT under the *in situ* conditions of Fig. 2c; C) Ni2p XPS spectra relative to Ni/HT under different gas atmospheres as indicated; d) EY Ni L_3-edges NEXAFS relative to Ni/HT under different gas atmosphere compared to Ni nanoparticles and as received Ni polycrystalline sample covered with C impurities; e) Ni2p XPS spectra for Ni-Fe/HT under the *in situ* condition of Fig. 2a. f) Fe2p XPS spectra for Ni-Fe/HT under the *in situ* conditions of Fig. 2a: the component relative to Fe(II) is found at a BE of 708.7 eV, whereas the Fe(III) species are found at a BE of 710.5 eV; g) EY Ni L-edges NEXAFS for the Ni-Fe/HT under the *in situ* conditions of Fig. 2a; h) EY C K-edge NEXAFS measured for Ni-Fe/HT under the *in situ* conditions of Fig. 2a; i) Ni L-edges NEXAFS of the Ni-Fe/HT under the *in situ* conditions of Fig. 2c; l) EY C K-edge NEXAFS measured for Ni/HT under the *in situ* conditions of Fig. 2c; m) Comparison of Ni L-edges spectra with detail of the P1 resonance in the inset during various tests as indicated in the legend; n) Absolute abundance of the elements determined by quantitative XPS analysis using homogeneous model distribution for the sample Ni/HT during tests reported in Fig. 2d; o) Absolute abundance of the elements determined by quantitative XPS analysis using homogeneous model distribution for the sample Ni-Fe/HT during tests reported in Fig. 2b.

Thermodynamic calculations

To compare the catalysts' performance to the theoretical thermodynamic limits, we calculated the equilibrium composition, conversion, selectivity and yields to CH_4 in the same conditions used for testing the Ni/HT and Ni-Fe/HT in situ. The equilibrium composition was calculated by using the Soave-Redlich-Kwong (SRK) equation of state (EOS) and the Gibbs free energy minimization method. The formation of carbon was also considered.

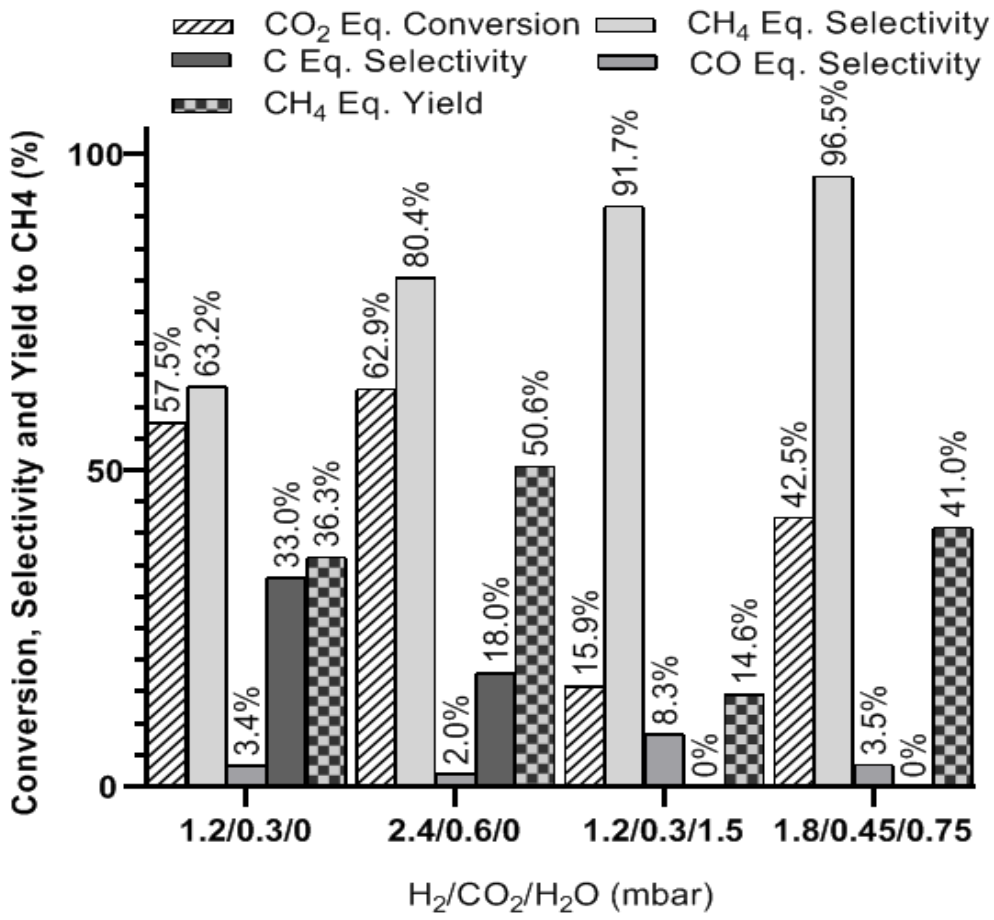

Figure S 4: Equilibrium calculations for the methanation reaction. Calculated by using Chemstations Chemcad 7.1.5, the Soave-Redlich-Kwong equation of state and Gibbs free energy minimization method at 300 °C (partial pressures reported in figure).

As shown in Fig. S4, in the absence of water in the reaction mixture, the equilibrium conversion and yield towards CH_4 increase with increasing of the total pressure from 1 to 3 mbar. Note that the formation of carbon is expected in the absence of water at such low pressures. In contrast, the equilibrium conversion to methane decreases with increasing of the partial pressure of water from 0 to 1.5 mbar. The expected trends of selectivity towards CO and deposited carbon at the equilibrium are opposite. Comparing the obtained conversion of CO_2 in the in-situ tests with the conversion expected by thermodynamic at the equilibrium, we see that the former is always lower than the latter one. However, Test 5 ($H_2/CO_2/H_2O$ 1.5/0.3/1.5) for the Ni/HT catalyst is an exception. In the latter case, the conversion was 19.4%, while, the thermodynamic prediction is consistent with a maximum equilibrium conversion of 15.9 %. This might be the result of a slight variation of the H_2/CO_2 ratio due to the experimental set-up.

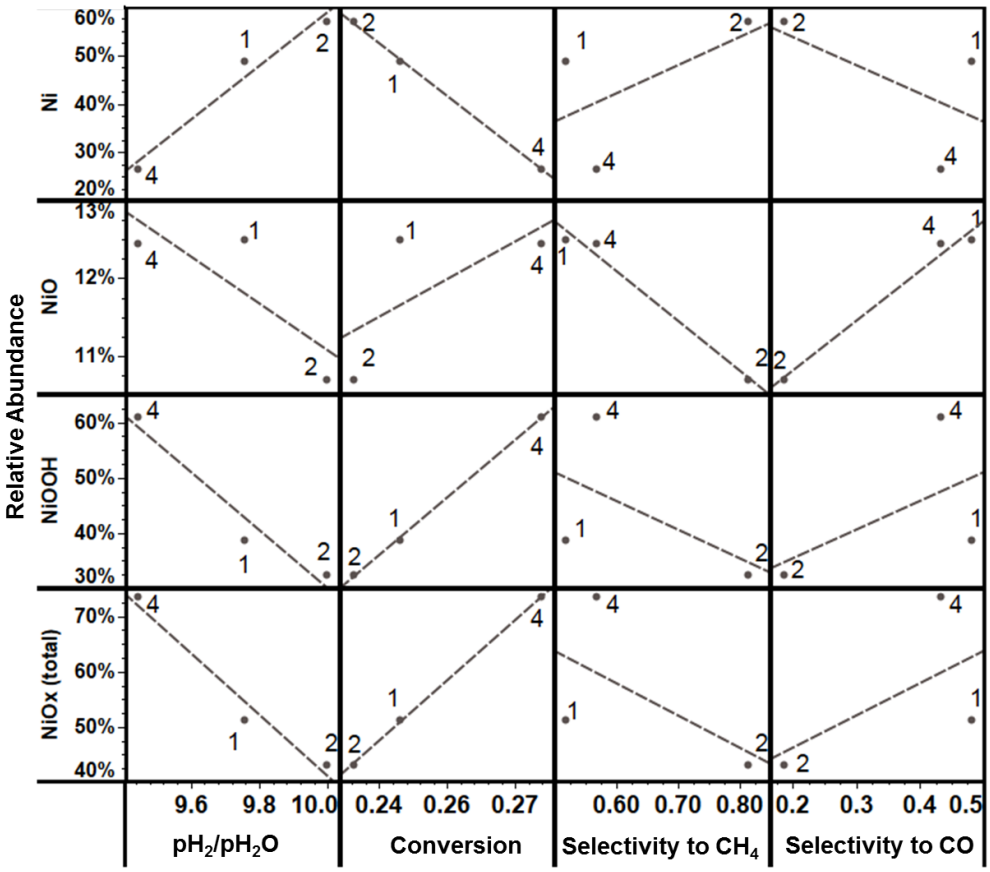

Figure S 5: Ni-Fe/HT: Correlations attempts between relative percentual abundance of Ni species (Ni0, NiO, NiOOH) measured in-situ at 300°C during Test 1 ($H_2/CO_2/H_2O$, 1.2/0.3/0 mbar), Test 2 ($H_2/CO_2/H_2O$, 2.4/0.6/0 mbar) and Test 4 ($H_2/CO_2/H_2O$, 2.4/0.6/0 mbar) by fitting the Ni 2p XPS peaks as a function of the measured pH_2/pH_2O, conversion, selectivity to CH_4 and CO (numerical labels in the figure indicate the number of the Test at which the above reported parameters were measured, dashed lines represent linear trend lines).